Radiology: Cardiothoracic Imaging

TECHNICAL DEVELOPMENT

# Compressed Sensing Cardiac Cine Imaging Compared with Standard Balanced Steady-State Free Precession Cine Imaging in a Pediatric Population

*Davide Curione, MD • Paolo Ciliberti, MD • Caterina Beatrice Monti, MD, PhD • Davide Capra, MD • Veronica Bordonaro, MD • Paolo Ciancarella, MD • Teresa Pia Santangelo, MD • Carmela Napolitano, MD • Dolores Ferrara, MD • Marco Alfonso Perrone, MD • Francesco Secchi, MD, PhD* • Aurelio Secinaro, MD**

From the Advanced Cardiovascular Radiology Unit, Department of Radiology and Bioimaging (D. Curione, V.B., P. Ciancarella, T.P.S., C.N., A.S.), and Department of Pediatric Cardiology and Cardiac Surgery (P. Ciliberti, M.A.P.), Bambino Gesù Children's Hospital IRCCS, Piazza Sant'Onofrio 4, 00165 Rome, Italy; Department of Biomedical Sciences for Health, Università degli Studi di Milano, Milan, Italy (C.B.M., D. Capra, F.S.); Department of Radiology, Santobono-Pausilipon Children's Hospital, Naples, Italy (D.F.); and Unit of Radiology, IRCCS Policlinco San Donato, San Donato Milanese, Italy (F.S.). Received April 18, 2021; revision requested June 22; revision received March 21, 2022; accepted March 29. **Address correspondence to** D. Curione (e-mail: *davide.curione@opbg.net*).

*F.S. and A.S. are co-senior authors.

Authors declared no funding for this work.

Conflicts of interest are listed at the end of this article.

*Radiology: Cardiothoracic Imaging* 2022; 4(2):e210109 • https://doi.org/10.1148/ryct.210109 • Content codes: CA MR PD

***Purpose:*** To compare real-time compressed sensing (CS) and standard balanced steady-state free precession (bSSFP) cardiac cine imaging in children.

***Materials and Methods:*** Twenty children (mean age, 15 years ± 5 [SD], range, 7–21 years; 10 male participants) with biventricular congenital heart disease ($n$ = 11) or cardiomyopathy ($n$ = 9) were prospectively included. Examinations were performed with 1.5-T imagers by using both bSSFP and CS sequences in all participants. Quantification of ventricular volumes and function was performed for all images by two readers blinded to patient diagnosis and type of sequence. Values were correlated with phase-contrast flow measurements by one reader. Intra- and interreader agreement were analyzed.

***Results:*** There were no significant differences between ventricular parameters measured on CS compared with those of bSSFP ($P >$ .05) for reader 1. Only ejection fraction showed a significant difference ($P$ = .02) for reader 2. Intrareader agreement was considerable for both sequences (bSSFP: mean difference range, +1 to −2.6; maximum CI, +7.9, −13; bias range, 0.1%–4.1%; intraclass correlation coefficient [ICC] range, 0.931–0.997. CS: mean difference range, +7.4 to −5.6; maximum CI, +37.2, −48.8; bias range, 0.5%–7.5%; ICC range, 0.717–0.997). Interreader agreement was acceptable but less robust, especially for CS (bSSFP: mean difference range, +2.6 to −5.6; maximum CI, +60.7, −65.3; bias range, 1.6%–6.2%; ICC range, 0.726–0.951. CS: mean difference range, +10.7 to −9.1; maximum CI, +87.5, −84.6; bias range, 1.1%–17.3%; ICC range, 0.509–0.849). The mean acquisition time was shorter for CS (20 seconds; range, 17–25 seconds) compared with that for bSSFP (160 seconds; range, 130–190 seconds) ($P <$ .001).

***Conclusion:*** CS cardiac cine imaging provided equivalent ventricular volume and function measurements with shorter acquisition times compared with those of bSSFP and may prove suitable for the pediatric population.



Cardiovascular MRI (CMR) is a key imaging modality in children, especially in congenital heart disease (CHD) (1–4). Evaluation of biventricular volumes and function is crucial in this setting. The standard CMR method to calculate these parameters entails multisection, cardiac-gated balanced steady-state free precession (bSSFP) cine imaging (5,6). Unfortunately, bSSFP cine sequences require multiple breath holds, which are time-consuming and can be difficult in young children with heart disease. Therefore, new emerging techniques aiming to reduce CMR imaging time are recently gaining increasing interest (7,8). However, data on this topic are scant in the pediatric population.

Compressed sensing (CS) is a relatively novel MRI technique based on k-space incoherent subsampling, paired with a noise-reduction algorithm employing sparse representation in a nonlinear iterative reconstruction process (9,10). The purpose is to drastically speed up acquisition time without significantly degrading image quality. In recent years, CS has become increasingly popular in CMR. This is especially true for cine imaging in adults, in which real-time CS has shown to be accurate and reproducible, allowing for fast and reliable imaging even in patients who may be difficult to image (11–14).

Compared with standard bSSFP cine sequences, the major advantages of CS are the decreased imaging duration and the relative insensitivity to motion artifacts, such as irregular heart rhythms and breathing (15). These features account for most of its appeal in the pediatric population, in which patient cooperation is often limited. Moreover, in contrast with classic real-time cine imaging using parallel imaging, real-time CS yields higher spatial and temporal resolution closer to that of standard bSSFP (16).

Recent experiences investigating CS in children and CHD are encouraging, showing feasibility and strong agreement with standard bSSFP cine imaging (17). In this context, we present results from our initial experience of

### Abbreviations

bSSFP = balanced steady-state free precession, CHD = congenital heart disease, CMR = cardiovascular MRI, CS = compressed sensing, EDV = end-diastolic volume, EF = ejection fraction, ESV = end-systolic volume, ICC = intraclass correlation coefficient, LV = left ventricle, RV = right ventricle, SV = stroke volume


### Summary

Compressed sensing cardiac cine imaging produces equivalent ventricular volume and function measurements with shorter acquisition times compared with standard steady-state free precession imaging and may prove suitable for the pediatric population.


### Key Points

- Compressed sensing (CS) cardiac cine imaging showed no significant differences ($P > .05$) for volume and function quantification compared with those from standard balanced steady-state free precession (bSSFP) evaluation performed by two readers in children affected by biventricular congenital heart disease or cardiomyopathies, except for ejection fraction assessment by one reader ($P = .02$).
- Intrareader agreement was considerable for both sequences, especially for bSSFP (bSSFP vs CS: mean difference range, +1 to −2.6 vs +7.4 to −5.6; maximum CI, +7.9, −13 vs +37.2, −48.8; bias range, 0.1%–4.1% vs 0.5%–7.5%; intraclass correlation coefficient [ICC] range, 0.931–0.997 vs 0.717–0.997); interreader agreement was acceptable but less robust, especially for CS (bSSFP vs CS: mean difference range, +2.6 to −5.6 vs +10.7 to −9.1; maximum CI, +60.7, −65.3 vs +87.5, −84.6; bias range, 1.6%–6.2% vs 1.1%–17.3%; ICC range, 0.726–0.951 vs 0.509–0.849).
- The mean acquisition time was shorter for CS (20 seconds; range, 17–25 seconds) compared with that of bSSFP (160 seconds; range, 130–190 seconds) ($P < .001$); on the other hand, the mean reconstruction time was longer for CS (120 seconds; range, 100–150 seconds) compared with an almost instant time for bSSFP (mean, 2 seconds; range, 0–5 seconds) ($P < .001$).


### Keywords

Compressed Sensing, Balanced Steady-State Free Precession, Cine Imaging, Cardiovascular MRI, Pediatrics, Cardiac, Heart, Cardiomyopathies, Congenital, Segmentation


how CS performs in comparison with that of standard bSSFP in a small group of pediatric patients.

## Materials and Methods

### Study Participants

We prospectively studied 20 consecutive pediatric participants (mean age, 15 years ± 5; range, 7–21 years; 10 male participants) who had either CHD treated with biventricular repair or cardiomyopathy and who were referred for CMR at our institution between January 2019 and March 2019. Adult patients with CHD (>18 years) and children with single ventricle physiology were excluded ($n = 8$). Institutional review board approval was obtained, and informed written consent for additional research scans was acquired from all individuals or guardians. All procedures were in accordance with the ethical standards of the responsible committee on human experimentation and with the Helsinki Declaration and its late amendments.

### CMR Image Acquisition

All imaging was performed with a 1.5-T MRI system (MAGNETOM Aera; Siemens Healthineers). A 16-element coil system for signal detection was used, consisting of posterior spine coils incorporated into the imaging table and one anterior phased-array body coil. A vector electrocardiographic system was employed for cardiac gating. Ventricular volume assessment was performed with both standard bSSFP and real-time CS cine sequences in the ventricular short-axis plane by using sufficient contiguous sections (mean, 15 sections, range, 12–18 sections) for gapless imaging to ensure whole coverage of both ventricles. Standard bSSFP cine imaging involved a multisection retrospectively cardiac-gated Cartesian sequence, with two sections acquired during every breath hold. The main imaging parameters were as follows: repetition time and echo time, 2.92 and 1.21 msec, respectively; rectangular field of view, 340 mm × 75%; matrix, 256 × 192; flip angle, 73°; bandwidth, 930 Hz/pixel; acceleration factor (generalized autocalibrating partially parallel acquisition), two; spatial resolution, 1.5 × 1.5 × 7 mm; temporal resolution, approximately 37 msec; and reconstructed cardiac phases, 25. Real-time CS cine imaging employed a multisection retrospectively cardiac-gated Cartesian sequence, with the whole volume acquisition being obtained during either a single breath hold or free breathing when breath holding was not feasible because of poor cooperation. The acquisition duration was two R-R intervals per section. The first heartbeat was a nonimaging "dummy" beat used to reach the steady state, whereas the second heartbeat was used for data acquisition. The main imaging parameters were as follows: repetition time and echo time, 2.66 and 1.1 msec, respectively; rectangular field of view, 360 mm × 75%; matrix, 208 × 156; flip angle, 55°; bandwidth, 962 Hz/pixel; acceleration factor (CS), 9.9; spatial resolution, 1.7 × 1.7 × 7 mm (8 mm in two cases); temporal resolution, approximately 40 msec; and reconstructed cardiac phases, 20. Because CS is a prototype sequence with many fixed and intertwined parameters, it was acquired by using the original settings given to our institution by the imager vendor to ensure reproducibility.

### CMR Image Analysis

Quantification of ventricular volumes and function were performed for all examinations by two readers from two different centers: a CMR and CHD fellowship-trained radiologist (reader 1, D. Curione, with 5 years of experience) and a CMR-focused radiology resident in training (reader 2, D. Capra, with 2 years of experience), respectively. Both readers were blinded to patient diagnosis and type of sequence and performed measurements in a random order by using commercially available software (cvi42; Circle Cardiovascular Imaging). Reader 1 measured all parameters twice, with a long interval between readings (>1 year). The end-diastolic and end-systolic phases were identified for each ventricle through simultaneous visual inspection of all short-axis cine images. The endocardial borders of all sections at the end diastole and the end systole were traced manually, including papillary muscles and trabeculation in the blood pool volume. End-diastolic volume (EDV), end-

systolic volume (ESV), stroke volume (SV) (SV = EDV – ESV), and ejection fraction (EF) (EF = SV/EDV × 100) were calculated. Reader 1 correlated cine values (systemic and pulmonary SV) with phase-contrast measurements (aortic and pulmonary valve flows, respectively), as is routine in our center—even with bSSFP sequences—to compensate for the lower resolution of CS and to maximize its benefits. On the other hand, reader 2 did not use this correlation to assess for reproducibility when removing this bias.

### Statistical Analysis

Continuous data were reported as means ± SDs. Categorical variables were reported as numbers and percentages. Student *t* test was used to compare continuous variables. A *P* value of less than .05 indicated statistical significance. A sample of 20 patients provides 80% power to detect an effect size of 0.67 based on a paired *t* test, assuming a two-tailed .05 alpha level (18). Bland-Altman analyses were used to evaluate the agreement between different sequences and readers, with results reported as mean differences along with CIs, and interpreted according to clinical relevance (19). Concordance was also appraised through the assessment of intraclass correlation coefficients (ICCs) calculated by using a two-way, random-effects model aiming for absolute agreement. Statistical analyses were performed by using Python version 7.18.1.

## Results

### Participant Characteristics

The mean participant age was 15 years ± 5 (range, 7–21 years). The mean height, weight, and body surface area were 148 cm ± 17 (range, 110–178 cm), 48 kg ± 17 (range, 26–72 kg), and 1.46 $m^2$ ± 0.33 (range, 0.9–2 $m^2$), respectively. Ten participants (50%) were male. Eleven participants had CHD (three with aortic coarctation, two with aortic stenosis, two with repaired tetralogy of Fallot, two with repaired transposition of the great arteries, one with congenitally corrected transposition of the great arteries, and one with aortopathy), whereas the rest had suspected or known cardiomyopathy (five with ectopic arrhythmia, one with hypertrophic cardiomyopathy, one with dilated cardiomyopathy, and one with myopericarditis) as diagnosed by referring cardiologists. The mean heart rate was 81 beats per minute ± 14 (range, 55–110 beats per minute). Two patients had frequent arrhythmia (ventricular extrasystole), whereas three patients had difficulty holding their breath during imaging.

### CMR Analysis

***Ventricular volumes and function.—*** We found no evidence of a statistically significant difference ($P > .05$) in left ventricular (LV) or right ventricular (RV) EDV, ESV, SV, and EF between CS and bSSFP for reader 1. Figure 1 shows the comparison of measurements obtained with the two sequences by reader 1. The mean difference between measurements was small and similar for LV and RV results (mean difference range, +6.83 to −1.61). CIs, on the other hand, were wider for volumes, particularly for the RV (maximum CI, +49.2, −35.54 for RV SV), and narrower for EF (maximum CI, +5.07, −6.61 for RV EF). For reader 2, only LV and RV EF showed significant differences (both $P = .02$). Ventricular measurements obtained with both sequences by both readers are summarized in Table 1.

***Intra- and interreader agreement.—*** Intrareader variability (reader 1) was characterized by negligible mean differences, contained CIs and bias, and high ICCs for both LV and RV measurements obtained with bSSFP sequences (mean difference range, +1 to −2.6; maximum CI, +7.9, −13 for RV EDV; bias range, 0.1%–4.1%; ICC range, 0.931–0.997). CS also showed small LV mean differences but wider CIs and bias and slightly lower ICCs, especially for RV values (mean difference range, +7.4 to −5.6; maximum CI, +37.2, −48.8 for RV EDV; bias range, 0.5%–7.5%; ICC range, 0.717–0.997).

Interreader agreement was acceptable but less robust for both sequences, with overall larger mean differences, wider CIs and bias, and lower ICCs for CS (bSSFP: mean difference range, +2.6 to −5.6; maximum CI, +60.7, −65.3 for RV EDV; bias range, 1.6%–6.2%; ICC range, 0.726–0.951. CS: mean difference range, +10.7 to −9.1; maximum CI, +87.5, −84.6 for LV EDV; bias range, 1.1%–17.3%; ICC range, 0.509–0.849). Intra- and interreader results are detailed in Table 2.

***Acquisition and reconstruction times.—*** The mean acquisition time of the entire stack of short-axis images was much shorter for CS (20 seconds; range, 17–25 seconds) compared with that of bSSFP (160 seconds; range, 130–190 seconds) ($P < .001$). On the other hand, the mean reconstruction time was quite long for CS, with an approximate mean value of 120 seconds (range, 100–150 seconds) to complete the whole volume compared with the almost instant time for bSSFP (mean, 2 seconds; range, 0–5 seconds) ($P < .001$).

## Discussion

In our study, we found no evidence of a difference in calculated ventricular volumes other than EF between real-time CS and standard bSSFP cine imaging. This suggests that CS is a valid alternative to bSSFP for volumetric analysis, despite the smaller anatomic structures and higher heart rates typically found in children and the complex ventricular geometry that often characterizes CHD (Figs 2, 3), in which usual cardiac anatomy can substantially be subverted and multiple lesions can exist simultaneously, requiring a high degree of definition and accuracy. From a clinical point of view, equivalent ventricular quantification between sequences is paramount for their implementation, irrespective of differences in other imaging parameters, as important biases may impact clinical decision making (17,20).

In our series, the data were more robust for reader 1, especially in terms of variability between measurements and sequences. In fact, for reader 2, there was a statistically significant difference in EF between the imaging sequences and higher interobserver variability. This discrepancy could be explained by taking into account that reader 1 had greater experience and used

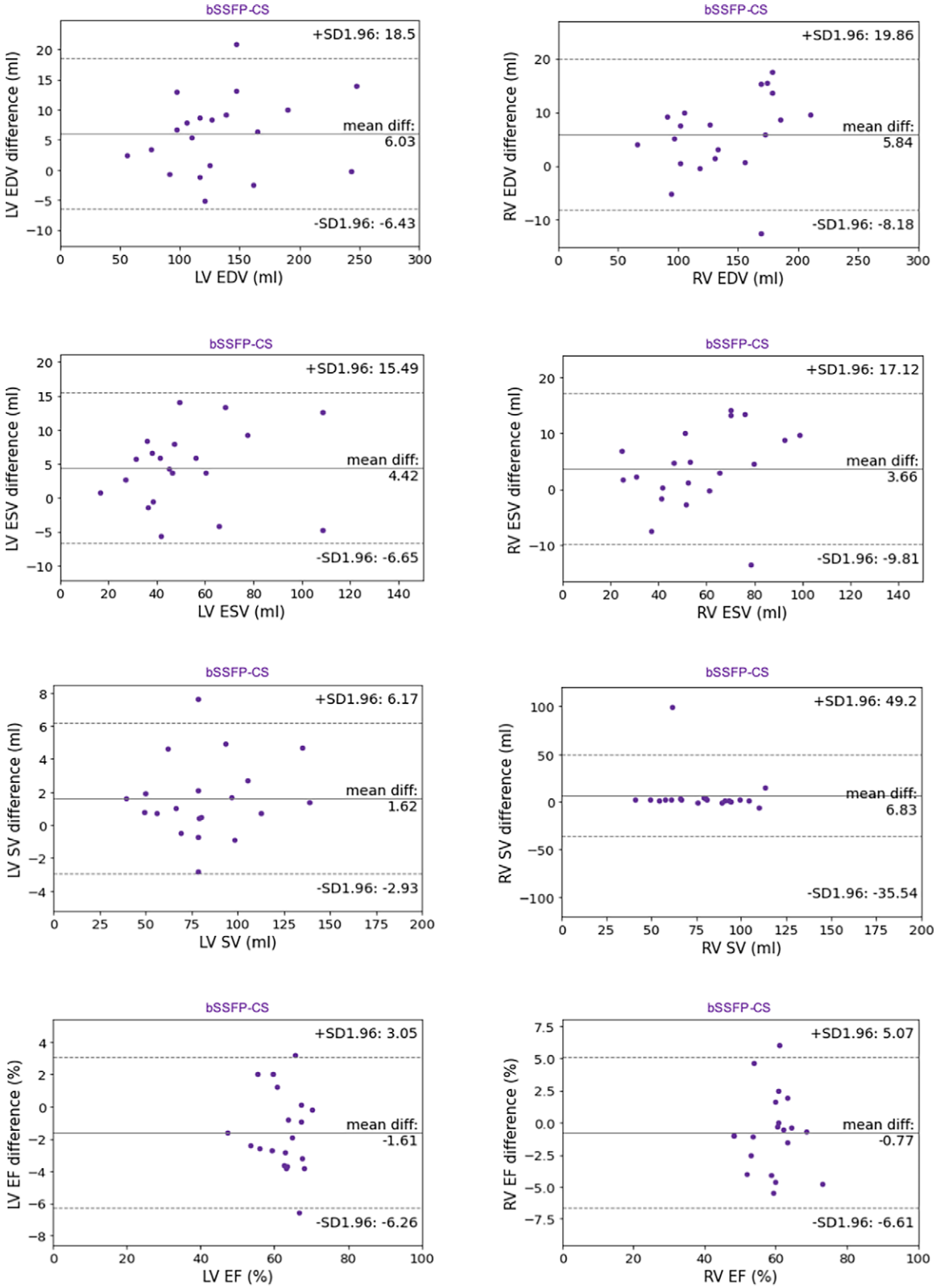


**Figure 1:** Bland-Altman plots compare measurements obtained with standard bSSFP and real-time CS cine imaging by reader 1. bSSFP = balanced steady-state free precession, CS = compressed sensing, EDV = end-diastolic volume, EF = ejection fraction, ESV = end-systolic volume, LV = left ventricle, RV = right ventricle, SV = stroke volume.

flow-volume correlation. Indeed, having more experience in the segmentation of ventricles and in pediatric imaging and CHD in general may have played a key role in the more consistent results obtained by reader 1, who was more accustomed to the images obtained in this type of patient. This could mean that the differences between the two readers may be related, at least to a certain

**Table 1: Ventricular Measurements Obtained with Standard bSSFP and Real-time CS Cine Imaging by Two Readers**

| | bSSFP | | CS | | *P* Value | |
|---|---|---|---|---|---|---|
| Measurement | R1 | R2 | R1 | R2 | R1 | R2 |
| LV EDV (mL) | 135.8 ± 48.1 | 140.3 ± 41.6 | 133.2 ± 50.2 | 130.5 ± 44.9 | .87 | .48 |
| LV ESV (mL) | 53.5 ± 24.9 | 55.2 ± 22.4 | 52.7 ± 27.6 | 60.2 ± 25.4 | .91 | .52 |
| LV SV (mL) | 82.5 ± 25.5 | 85.0 ± 24.8 | 80.7 ± 25.3 | 70.3 ± 24.6 | .82 | .07 |
| LV EF (%) | 61.6 ± 7 | 61.1 ± 9.1 | 61.9 ± 7.4 | 54.0 ± 9.3 | .9 | .02* |
| RV EDV (mL) | 140.2 ± 39.9 | 143.2 ± 42.6 | 134.6 ± 37.3 | 132.7 ± 45.0 | .6 | .46 |
| RV ESV (mL) | 59.5 ± 21.6 | 56.5 ± 22.9 | 55.9 ± 19.6 | 61.5 ± 25.9 | .58 | .53 |
| RV SV (mL) | 80.9 ± 21.2 | 86.6 ± 25.3 | 74.3 ± 24.2 | 71.2 ± 24.4 | .36 | .06 |
| RV EF (%) | 58.5 ± 6.4 | 61.0 ± 8.8 | 59.1 ± 6.7 | 53.9 ± 8.9 | .79 | .02* |

Note.—Ventricular measurements are expressed as mean ± SD. bSSFP = balanced steady-state free precession, CS = compressed sensing, EDV = end-diastolic volume, EF = ejection fraction, ESV = end-systolic volume, LV = left ventricle, R1 = reader 1, R2 = reader 2, RV = right ventricle, SV = stroke volume.
* Indicates statistical significance ($P < .05$).

**Table 2: Intra- and Interreader Variability and Reliability for Standard bSSFP and Real-time CS Cine Imaging**

| | Intrareader | | | | Interreader | | | |
|---|---|---|---|---|---|---|---|---|
| | bSSFP | | CS | | bSSFP | | CS | |
| Measurement | BA | ICC | BA | ICC | BA | ICC | BA | ICC |
| LV EDV (mL) | −2.1 (+7.9, −12.1), 1.5 | 0.997 | +0.9 (+14.4, −12.7), 0.7 | 0.995 | −5.6 (+58.1, −68.6), 4.1 | 0.858 | +1.5 (+87.5, −84.6), 1.1 | 0.739 |
| LV ESV (mL) | −2.2 (+7.2, −11.6), 4.1 | 0.991 | +1.3 (+14, −11.3), 2.5 | 0.984 | −3.3 (+16.9, −23.5), 6.2 | 0.951 | −9.1 (+32.9, −51.2), 17.3 | 0.802 |
| LV SV (mL) | +0.1 (+5.6, −5.6), 0.1 | 0.997 | −0.4 (+5.6, −6.5), 0.5 | 0.997 | −2 (+44.1, −48.1), 2.4 | 0.731 | +10.7 (+60.5, −39.1), 13.3 | 0.661 |
| LV EF (%) | +1 (+7.2, −5.2), 1.6 | 0.931 | −0.5 (+5.7, −6.7), 0.8 | 0.937 | +1.4 (+12.5, −9.7), 2.3 | 0.854 | +8.5 (+20.4, −3.3),13.7 | 0.829 |
| RV EDV (mL) | −2.6 (+7.9, −13), 1.9 | 0.996 | +7.4 (+48.3, −33.6), 5.5 | 0.930 | −2.3 (+60.7, −65.3), 1.6 | 0.826 | +2.4 (+61.8, −57.1), 1.8 | 0.849 |
| RV ESV (mL) | −1.7 (+8.5, −11.8), 2.9 | 0.987 | +3.4 (+15.1, −8.4), 6.1 | 0.979 | +2.6 (+43.3, −38.2), 4.4 | 0.729 | −6 (+34.5, −46.5), 10.7 | 0.749 |
| RV SV (mL) | −0.9 (+4.8, −6.7), 1.1 | 0.996 | −5.6 (37.2, −48.8), 7.5 | 0.717 | −4.8 (+27.3, −36.9), 5.9 | 0.860 | +3.7 (+61.1, −53.7), 5.0 | 0.509 |
| RV EF (%) | +0.2 (+5.3, −4.8), 0.3 | 0.957 | −2.3 (+6.1, −10.6), 3.9 | 0.885 | −2.2 (+11.7, −16), 3.8 | 0.726 | +5.7 (+22.2, −10.8), 9.6 | 0.566 |

Note.—Bland-Altman values are expressed as mean difference, with limits of agreement from +1.96 second to −1.96 second in parentheses, followed by percentages of the mean volumes and function. ICCs are expressed as numbers. BA = Bland-Altman, bSSFP = balanced steady-state free precession, CS = compressed sensing, EDV = end-diastolic volume, EF = ejection fraction, ESV = end-systolic volume, ICC = intraclass correlation coefficient, LV = left ventricle, RV = right ventricle, SV = stroke volume.

extent, to the observer rather than to the imaging technique. Moreover, the comparison of phase-contrast and volumetric values could further account for and enhance the discrepancies. Although there is clearly a bias, we decided to use flow-volume correspondence for one reader because it is part of everyday clinical practice in one center and is frequently described in children and CHD (2). We believe that whatever difficulty could be encountered in accurate ventricular segmentation with CS, due to

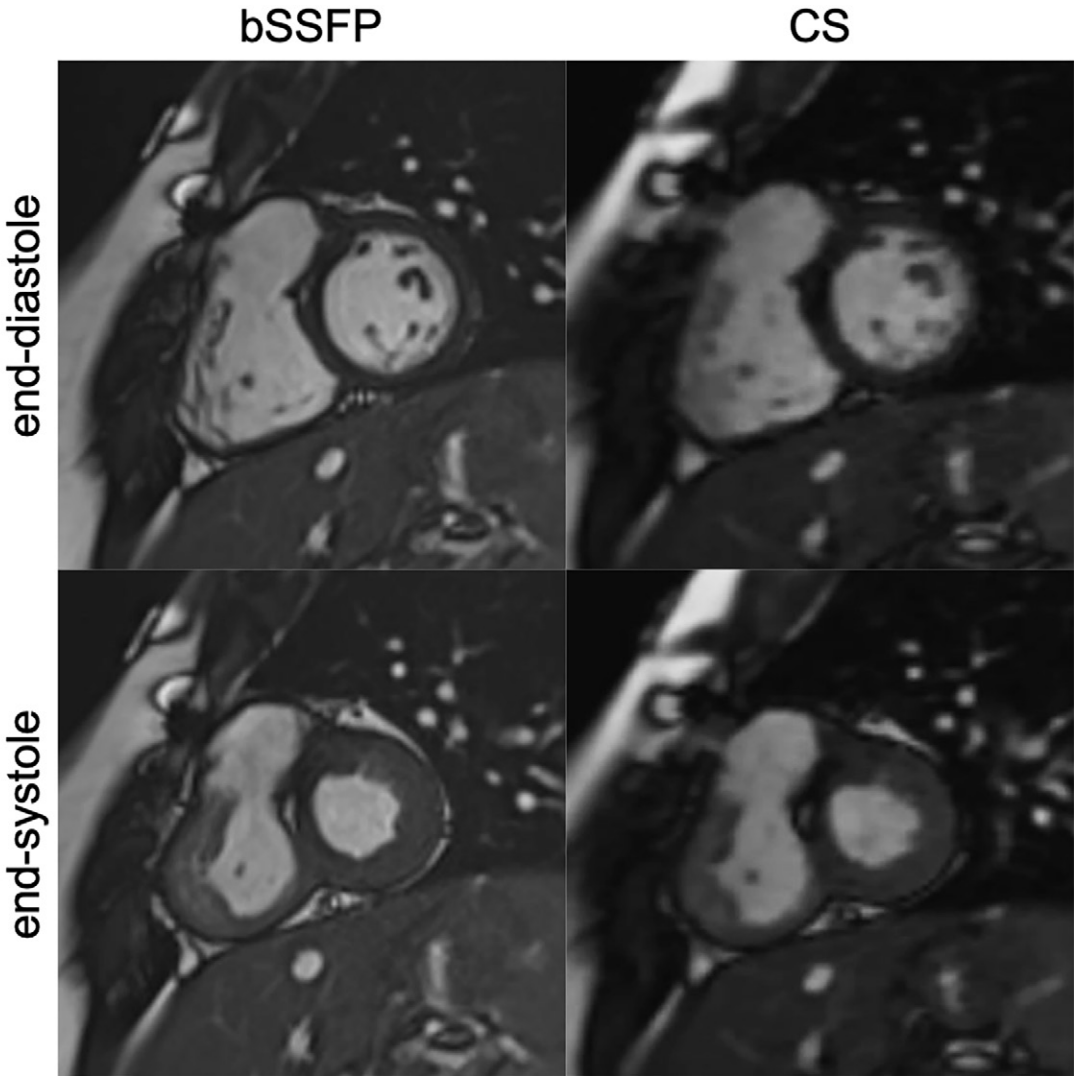


**Figure 2:** End-diastolic (top row) and end-systolic (bottom row) midventricular short-axis frames of standard bSSFP (left column) and real-time CS (right column) cine MRI sequences in a 13-year-old male patient with tetralogy of Fallot treated with transannular patch and ventricular septal defect closure. The chemical shift artifact at the anterobasal interventricular septum corresponds to the area of ventricular septal defect repair. bSSFP = balanced steady-state free precession, CS = compressed sensing.

known intrinsic lower image quality of the sequence (11,17), was substantially mitigated by these two aspects. Moreover, in certain specific cases, intrinsic imaging characteristics of CS may have led to greater differences in functional parameters between CS and bSSFP, especially for the RV. Hence, higher biases and limits of agreement may also be due to individual instances in which CS proved less reliable than cine, and future studies might aim at abating this issue via image quality appraisal. Besides, image quality was not the focus of our analysis and may vary depending on the type of CS sequence employed, with spiral k-space trajectories showing higher quality compared with that of Cartesian acquisition (12,17) and with more recent CS sequences showing analogous image quality compared with that of bSSFP imaging (21,22). In our study, Cartesian acquisition was chosen because it was one of the many fixed parameters of CS imaging. In any case, it is interesting to highlight that, even without flow-volume correlation, there was no evidence of a difference for all other ventricular parameters except EF, and mean differences between measurements were still reasonable despite having wide CIs, suggesting that CS sequences favor accuracy over precision.

In addition, CS entailed shorter acquisition times. This is a major advantage of CS over bSSFP, with predictable repercussions in terms of examination feasibility, tolerability, and scheduling. Because images can be obtained faster, CMR becomes easier and quicker, relying less on patient cooperation and rhythm regularity, saving time to image even more patients, and potentially reducing the need for anesthesia in smaller children. As an example, in our participants in whom irregular heart rhythm or difficulties in breath holding caused mild motion artifacts on bSSFP images, free-breathing CS provided artifact-free images for volume quantification (Fig 4).

On the other hand, technical obstacles, such as availability as a prototype sequence or long reconstruction times, could be an obstacle for the adoption of CS in everyday clinical

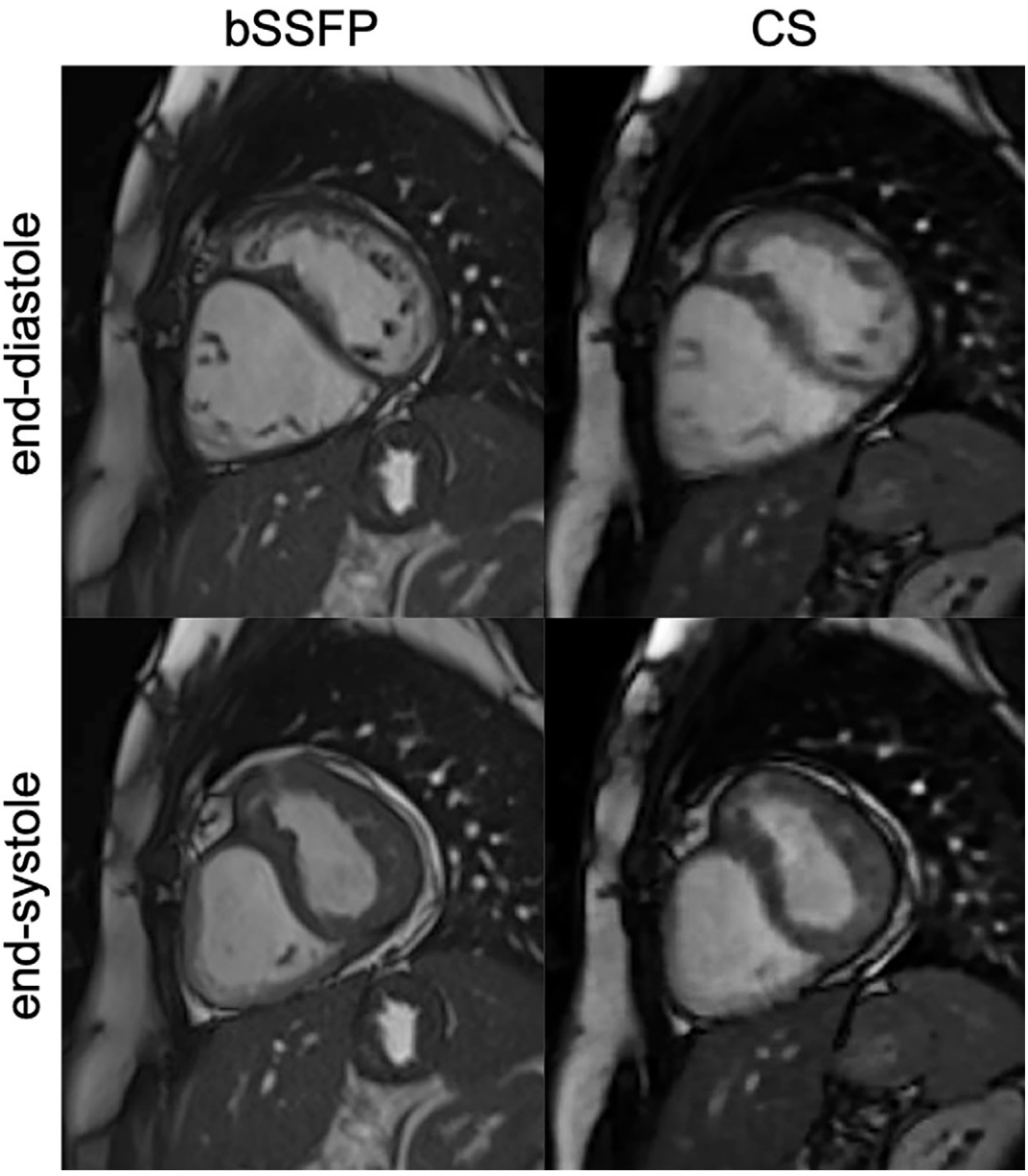


**Figure 3:** End-diastolic (top row) and end-systolic (bottom row) midventricular short-axis frames of standard bSSFP (left column) and real-time CS (right column) cine MRI sequences in a 15-year-old female patient with congenitally corrected transposition of the great arteries. The anterior chamber is the subpulmonary left ventricle, which is dilated due to the presence of an ostium secundum interatrial defect (not shown), whereas the posterior chamber is the hypertrophic systemic right ventricle. bSSFP = balanced steady-state free precession, CS = compressed sensing.

practice. The latter might partially be explained by the reconstruction of an additional interpolated series, based on the concept that because adjacent sections are structurally similar, it is possible to increase image quality by interpolating missing k-space data by using information from the neighboring sections (23). In any case, it is our belief that future technical advances will soon lessen, if not eliminate, these problems.

Our results were in line with those of other experiences reported in the literature (17,21,22). In our study, both children with CHD and children with cardiomyopathy were analyzed (17,21), retrospective gating was used (22), and the relevance of flow-volume correlation and experience were underlined.

## Study Limitations

Our pediatric cohort was numerically small, with a potential risk for selection and recall bias. In addition, the sample was heterogeneous with widely different ages and conditions. However, we were able to demonstrate that the advantages of CS apply to all groups. Nevertheless, we did not include patients with functionally single ventricle. Moreover, as this study was focused on the assessment of the agreement between CS and bSSFP cine imaging, we did not appraise correlations among different functional LV and RV parameters. Nevertheless, such correlations are already well known in the literature with different imaging modalities (24,25), and we may expect similar results from CS imaging once accuracy is ensured. Future stud-

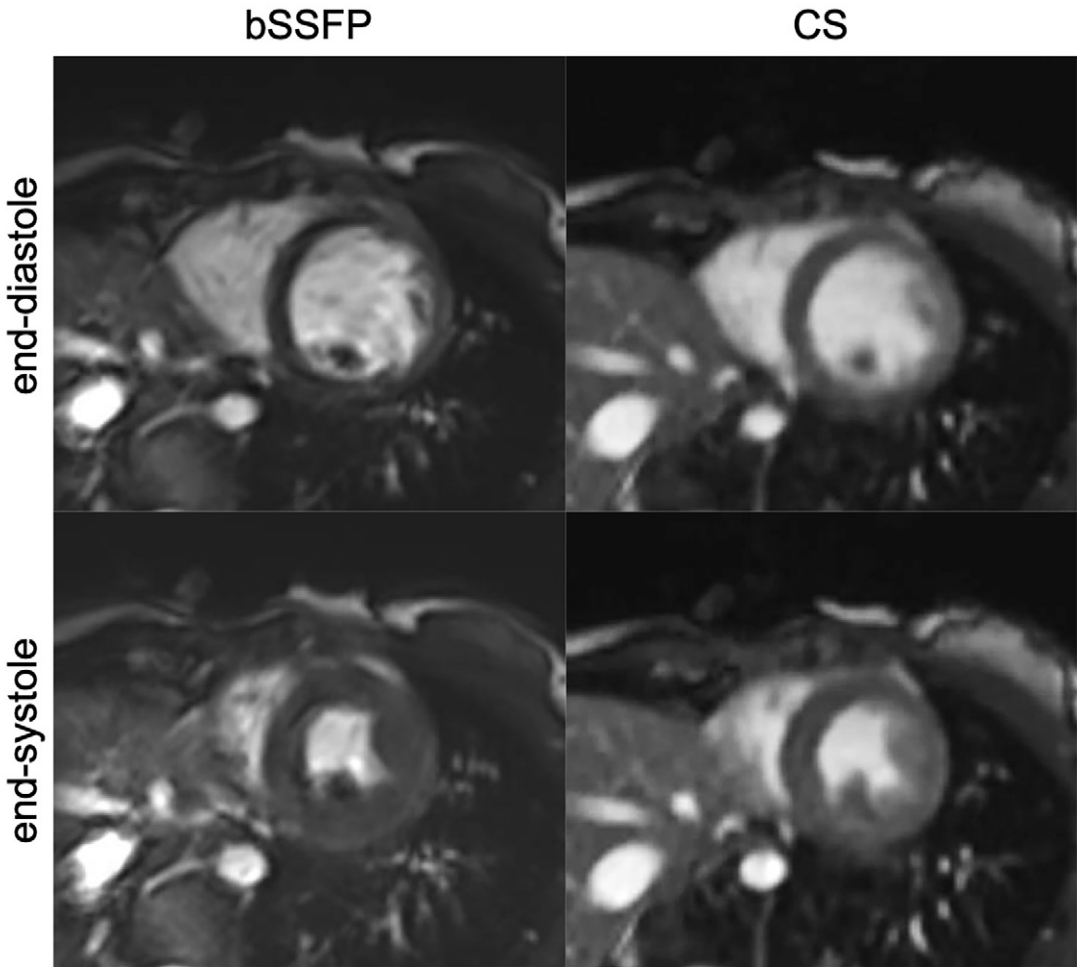


**Figure 4:** End-diastolic (top row) and end-systolic (bottom row) midventricular short-axis frames of standard bSSFP (left column) and real-time CS (right column) cine MRI sequences in a 9-year-old girl with sporadic ventricular ectopic beats and occasional difficulty performing breath holds. Standard bSSFP images show mild motion artifacts, whereas real-time CS frames are artifact free. bSSFP = balanced steady-state free precession, CS = compressed sensing.

ies on larger and more homogeneous groups of patients could provide more robust results.

## Conclusion

Our experience suggests that CS cardiac cine imaging is equivalent to bSSFP for the quantification of ventricular volumes and function with shorter acquisition times and may prove to be suitable for the pediatric population.

**Author contributions:** Guarantors of integrity of entire study, **D. Curione, P. Ciliberti, P. Ciancarella, C.N., A.S.**; study concepts/study design or data acquisition or data analysis/interpretation, all authors; manuscript drafting or manuscript revision for important intellectual content, all authors; approval of final version of submitted manuscript, all authors; agrees to ensure any questions related to the work are appropriately resolved, all authors; literature research, **D. Curione, P. Ciliberti, V.B., P. Ciancarella, T.P.S., C.N., D.F., M.A.P., F.S., A.S.**; clinical studies, **D. Curione, P. Ciliberti, V.B., C.N., D.F., A.S.**; statistical analysis, **P. Ciliberti, C.B.M., V.B., T.P.S., C.N., A.S.**; and manuscript editing, all authors

**Disclosures of conflicts of interest: D. Curione** No relevant relationships. **P. Ciliberti** No relevant relationships. **C.B.M.** No relevant relationships. **D. Capra** No relevant relationships. **V.B.** No relevant relationships. **P. Ciancarella** No relevant relationships. **T.P.S.** No relevant relationships. **C.N.** No relevant relationships. **D.F.** No relevant relationships. **M.A.P.** No relevant relationships. **F.S.** No relevant relationships. **A.S.** No relevant relationships.

## References

1. Valsangiacomo Buechel ER, Grosse-Wortmann L, Fratz S, et al. Indications for cardiovascular magnetic resonance in children with congenital and acquired heart disease: an expert consensus paper of the Imaging Working Group of the AEPC and the Cardiovascular Magnetic Resonance Section of the EACVI. Eur Heart J Cardiovasc Imaging 2015;16(3):281–297.
2. Fratz S, Chung T, Greil GF, et al. Guidelines and protocols for cardiovascular magnetic resonance in children and adults with congenital heart disease: SCMR expert consensus group on congenital heart disease. J Cardiovasc Magn Reson 2013;15(1):51.
3. Schicchi N, Secinaro A, Muscogiuri G, et al. Multicenter review: role of cardiovascular magnetic resonance in diagnostic evaluation, preprocedural planning and follow-up for patients with congenital heart disease. Radiol Med (Torino) 2016;121(5):342–351.
4. Muscogiuri G, Secinaro A, Ciliberti P, Fuqua M, Nutting A. Utility of cardiac magnetic resonance imaging in the management of adult congenital heart disease. J Thorac Imaging 2017;32(4):233–244.
5. Kawel-Boehm N, Maceira A, Valsangiacomo-Buechel ER, et al. Normal values for cardiovascular magnetic resonance in adults and children. J Cardiovasc Magn Reson 2015;17(1):29.
6. Kramer CM, Barkhausen J, Flamm SD, Kim RJ, Nagel E; Society for Cardiovascular Magnetic Resonance Board of Trustees Task Force on Standardized Protocols. Standardized cardiovascular magnetic resonance (CMR) protocols 2013 update. J Cardiovasc Magn Reson 2013;15(1):91.
7. Salerno M, Sharif B, Arheden H, et al. Recent advances in cardiovascular magnetic resonance: techniques and applications. Circ Cardiovasc Imaging 2017;10(6):e003951.

8. Kim D, Dyvorne HA, Otazo R, Feng L, Sodickson DK, Lee VS. Accelerated phase-contrast cine MRI using k-t SPARSE-SENSE. Magn Reson Med 2012;67(4):1054–1064.
9. Jaspan ON, Fleysher R, Lipton ML. Compressed sensing MRI: a review of the clinical literature. Br J Radiol 2015;88(1056):20150487.
10. Hollingsworth KG. Reducing acquisition time in clinical MRI by data undersampling and compressed sensing reconstruction. Phys Med Biol 2015;60(21):R297–R322.
11. Kido T, Kido T, Nakamura M, et al. Compressed sensing real-time cine cardiovascular magnetic resonance: accurate assessment of left ventricular function in a single-breath-hold. J Cardiovasc Magn Reson 2016;18(1):50.
12. Haji-Valizadeh H, Rahsepar AA, Collins JD, et al. Validation of highly accelerated real-time cardiac cine MRI with radial k-space sampling and compressed sensing in patients at 1.5T and 3T. Magn Reson Med 2018;79(5):2745–2751.
13. Vermersch M, Longère B, Coisne A, et al. Compressed sensing real-time cine imaging for assessment of ventricular function, volumes and mass in clinical practice. Eur Radiol 2020;30(1):609–619.
14. Vincenti G, Monney P, Chaptinel J, et al. Compressed sensing single-breath-hold CMR for fast quantification of LV function, volumes, and mass. JACC Cardiovasc Imaging 2014;7(9):882–892.
15. Goebel J, Nensa F, Schemuth HP, et al. Real-time SPARSE-SENSE cine MR imaging in atrial fibrillation: a feasibility study. Acta Radiol 2017;58(8):922–928.
16. Voit D, Zhang S, Unterberg-Buchwald C, Sohns JM, Lotz J, Frahm J. Real-time cardiovascular magnetic resonance at 1.5 T using balanced SSFP and 40 ms resolution. J Cardiovasc Magn Reson 2013;15(1):79.
17. Steeden JA, Kowalik GT, Tann O, Hughes M, Mortensen KH, Muthurangu V. Real-time assessment of right and left ventricular volumes and function in children using high spatiotemporal resolution spiral bSSFP with compressed sensing. J Cardiovasc Magn Reson 2018;20(1):79.
18. Staffa SJ, Zurakowski D. Statistical power and sample size calculations: a primer for pediatric surgeons. J Pediatr Surg 2020;55(7):1173–1179.
19. Bland JM, Altman DG. Statistical methods for assessing agreement between two methods of clinical measurement. Lancet 1986;1(8476):307–310.
20. Oosterhof T, van Straten A, Vliegen HW, et al. Preoperative thresholds for pulmonary valve replacement in patients with corrected tetralogy of Fallot using cardiovascular magnetic resonance. Circulation 2007;116(5):545–551.
21. Naresh NK, Malone L, Fujiwara T, et al. Use of compressed sensing to reduce scan time and breath-holding for cardiac cine balanced steady-state free precession magnetic resonance imaging in children and young adults. Pediatr Radiol 2021;51(7):1192–1201.
22. Hatipoglu S, Gatehouse P, Krupickova S, et al. Reliability of pediatric ventricular function analysis by short-axis "single-cycle-stack-advance" single-shot compressed-sensing cines in minimal breath-hold time. Eur Radiol 2022;32(4):2581–2593.
23. Pang Y, Zhang X. Interpolated compressed sensing for 2D multiple slice fast MR imaging. PLoS One 2013;8(2):e56098.
24. Friedberg MK, Su X, Tworetzky W, Soriano BD, Powell AJ, Marx GR. Validation of 3D echocardiographic assessment of left ventricular volumes, mass, and ejection fraction in neonates and infants with congenital heart disease: a comparison study with cardiac MRI. Circ Cardiovasc Imaging 2010;3(6):735–742. [Published correction appears in Circ Cardiovasc Imaging 2011;4(2):e4.]
25. Papavassiliou DP, Parks WJ, Hopkins KL, Fyfe DA. Three-dimensional echocardiographic measurement of right ventricular volume in children with congenital heart disease validated by magnetic resonance imaging. J Am Soc Echocardiogr 1998;11(8):770–777.